HHS Public Access

Author manuscript

Biomaterials. Author manuscript; available in PMC 2016 July 01.

Published in final edited form as:

Biomaterials. 2015 July ; 55: 119–128. doi:10.1016/j.biomaterials.2015.03.026.

Engineered heart slices for electrophysiological and contractile studies

Adriana Blazeski[1], **Geran M. Kostecki**[1], and **Leslie Tung**[*]

Department of Biomedical Engineering, The Johns Hopkins University, Baltimore, MD, USA

Abstract

A major consideration in the design of engineered cardiac tissues for the faithful representation of physiological behavior is the recapitulation of the complex topography and biochemistry of native tissue. In this study we present engineered heart slices (EHS), which seed neonatal rat ventricular cells (NRVCs) onto thin slices of decellularized cardiac tissue that retain important aspects of native extracellular matrix (ECM). To form EHS, rat or pig ventricular tissue was sectioned into 300 μm-thick, 5 to 16 mm-diameter disks, which were subsequently decellularized using detergents, spread on coverslips, and seeded with NRVCs. The organized fiber structure of the ECM remained after decellularization and promoted cell elongation and alignment, resulting in an anisotropic, functional tissue that could be electrically paced. Contraction decreased at higher pacing rates, and optical mapping revealed electrical conduction that was anisotropic with a ratio of approximately 2.0, rate-dependent shortening of the action potential and slowing of conduction, and lidocaine (sodium channel blocker)-induced slowing of conduction. Reentrant arrhythmias could also be pace-induced and terminated. EHS constitute an attractive *in vitro* cardiac tissue in which cardiac cells are cultured on thin slices of decellularized cardiac ECM that provide important biochemical, structural, and mechanical cues absent in traditional cell cultures.

Keywords

Cardiac tissue engineering; Extracellular matrix; Electrophysiology; Cell culture; Scaffold

1. Introduction

The field of cardiac tissue engineering has made steady progress over the past two decades. It is fueled not only by the prospect of myocardial repair [1,2] but also by the opportunity to develop new functional *in vitro* models that are physiologically relevant [1–3]. Various strategies have been employed in the fabrication of functional cardiac preparations that mimic native myocardium [1,2]. However, significant challenges remain in the ability of present engineered tissues to recapitulate the complex biochemical and biomechanical environment in native myocardium.

[*]Corresponding author. Department of Biomedical Engineering, The Johns Hopkins University, 720 Rutland Ave, Baltimore, MD, 21205, USA. Tel.: +1 410 955, 9603, ltung@jhu.edu (L. Tung).

[1]These authors contributed equally to this work.

Appendix A. Supplementary data

Supplementary data related to this article can be found at http://dx.doi.org/10.1016/j.biomaterials.2015.03.026.

Decellularization of whole organs has provided a natural scaffold that can be repopulated with a variety of cell types. Decellularized myocardial matrix has been successfully obtained by whole-heart perfusion [4,5] or through treatment of mm-thick sections of myocardium [6], and shown to provide a biocompatible substrate for cellular attachment while largely preserving matrix composition, organization, and mechanical properties. Cardiomyocytes cultured on this native matrix survive [7,8], contract [6], and respond to electrical stimulation [4,9,10]. Thus, decellularized myocardium is proving advantageous for the maintenance of cardiomyocytes and is receiving increasing attention as a scaffolding material for cardiac tissue engineering. Despite this progress, recellularization of three-dimensional native tissue remains a challenging proposition, particularly in the whole organ. On the other hand, recellularization of smaller and thinner tissues should be easier to achieve. With this approach in mind, our objective was to develop a physiological tissue system that supports cardiomyocyte survival and organization at confluent densities, contracts, and exhibits electrical conduction, anisotropic properties, and tissue-level arrhythmias.

2. Methods

An extended description of the methods is available in the supplementary material.

2.1. Preparation of decellularized slices

For slices made from rat ECM, adult rat hearts were suspended on a Langendorff perfusion setup and rinsed with double-distilled water (ddH_2O) to remove blood and assist in cell lysis via osmotic pressure. After removal of the atria, the ventricles were embedded in 4% low gelling temperature agarose and sectioned into 300 μm-thick slices using a vibratome (7000 smz, Campden Instruments, Lafayette, IN) before being cut with a hollow punch to the desired diameter (5–8 mm). For slices made from pig ECM, cylindrical plugs of myocardial tissue were punched out of the excised left ventricle of hearts from slaughterhouse pigs using a 14 mm or a 16 mm-diameter hollow punch. Plugs were stored at −80 °C for a minimum of 16 h. To obtain thin sections for decellularization, plugs were partially thawed, and an epicardial portion ~1 cm thick was cut out, embedded in agarose, and sliced 300 μm-thick using a vibratome. In this report, “native” slices refer to tissue slices prepared in this way and stored in PBS instead of undergoing decellularization.

Slices from rat and pig ECM were decellularized using SDS and Triton X-100 in a procedure modified from Ott et al. [4]. All solutions contained 1% antibiotic-antimycotic and 1% penicillin/streptomycin. The decellularized slices were carefully spread on sterilized plastic 5 mm-diameter coverslips (for rat ECM), or 14 mm-diameter coverslips (for pig ECM), and the outer perimeter of each slice was hooked around the edges of the coverslip. Coverslips with affixed slices were placed in 15 mm-diameter wells of standard 24-well culture plates and kept in sterile PBS or HBSS until use.

2.2. Seeding of decellularized slices with neonatal rat ventricular cells (NRVCs)

All animal procedures were performed in compliance with guidelines set by the Johns Hopkins Committee on Animal Care and Use and all federal and state laws and regulations.

Two million NRVCs were seeded in each well of a 24-well culture plate containing a single decellularized slice, to form an engineered heart slice (EHS). Day 0 of culture was defined to begin at the time of NRVC plating. After 18 h, EHS were washed with warm PBS, and fresh medium with 10% serum was added. On day 2, serum in the culture medium was reduced to 2% to inhibit non-cardiomyocyte proliferation, and cells were fed with 2% serum every other day thereafter.

2.3. Tissue characterization

Native and decellularized slices of pig ECM were dessicated, weighed, and digested in Tris EDTA containing 1% SDS and 1% Proteinase K by volume. Since the decellularized slices weighed much less than the native slices, ten decellularized slices were combined for more accurate weighing and DNA quantification. After digestion, DNA was isolated and quantified by measuring absorbance in a spectrophotometer (NanoDrop 1000, NanoDrop products, Wilmington, DE).

For mechanical testing, 30 mm-diameter, 300 μm-thick slices were prepared from pig left ventricle as described earlier, and a 1 cm-wide strip was cut from the center of each slice along the fiber direction. Native and decellularized samples were mounted on an EnduraTEC ELF 3200 Series instrument (Bose ElectroForce, Eden Prairie MN) by clamping each end, leaving a 1 cm initial length between the clamps. Samples were stretched uniaxially to 40% strain, in increments of 5% strain.

Slices of native and decellularized pig ECM were imaged by second harmonic generation (SHG). Native and decellularized slices from pig ECM were also frozen at −20 °C in optimal cutting temperature media, and 10 μm-thick cross-sections were cut every millimeter with a cryostat. These sections were imaged using a phase contrast microscope, and the cross-sectional thickness was measured using a custom MATLAB script.

Live cells in EHS made from pig ECM were imaged after staining using a viability/cytotoxicity kit 7 days after plating. Live cells were also imaged in combination with SHG to visualize cell locations relative to the matrix. For this, cells were additionally stained with either cell-impermeant ethidium homodimer-1 to image dead cell nuclei or cell-permeant DRAQ5 to image live cell nuclei. A z-stack of images was created, and the intensity of calcein-AM, DRAQ5 and SHG at each z-level, normalized to the maximum intensity for each stain, was plotted using a custom MATLAB script.

F-actin, DNA, collagen I, collagen III, and laminin in fixed native and decellularized slices of ECM, as well as cardiac troponin I (cTnI), α-actinin, connexin 43 (Cx43), and nuclei in fixed EHS, were stained using standard fixation and staining techniques and imaged using a confocal microscope. Nuclear elongation and alignment in EHS were analyzed using a custom MATLAB script.

2.4. Contraction measurement

During culture, the spontaneous beating condition of EHS made with pig ECM was recorded daily. For quantitative measurements of contractility, EHS from pig ECM were placed on a 37 °C heated stage in a 35 mm dish filled with Tyrode's solution 5 days after seeding. A

section of the EHS was unhooked from the coverslip so that it could move freely. The EHS was paced at 1–5 Hz, and the free region was imaged by a CCD camera. A custom MATLAB script was used to segment the image and calculate the mean displacement of the edge of the EHS over time, which was used as a surrogate for contractility to measure the force-frequency relationship of the EHS.

2.5. Electrophysiological studies

Most EHS were optically mapped 5–8 days after seeding. Some EHS made from pig ECM were mapped 21 days after seeding. EHS from rat ECM were placed in Tyrode's solution in a 35 mm dish and stained with 10 μM of the voltage-sensitive dye di-4-ANEPPS for 10 min. This solution was then removed from the dish, and replaced with Tyrode's solution containing 10 μM of the contraction inhibitor blebbistatin. At least 10 min after adding blebbistatin, the EHS were field stimulated and optically mapped using a CMOS camera (MiCAM Ultima-L, SciMedia).

EHS from pig ECM was optically mapped using a custom optical fiber system and protocol described previously [11]. Briefly, EHS were placed in the mapping chamber and treated with 20 μM di-4-ANEPPS and 10 μM blebbistatin in Tyrode's solution for 10 min. Tyrode's solution (35 ± 1 °C) containing 10 μM blebbistatin was then continuously perfused through the chamber for the duration of each experiment to inhibit motion artifacts. The stimulus threshold voltage was determined at 2 Hz, and a voltage 10% higher was used for experiments. EHS were paced at 2 Hz, then in increments of 1 Hz up to 5 Hz, and then in smaller increments until loss of capture. Some EHS were challenged with stepwise increasing doses of lidocaine ranging from 90 μM to 360 μM and paced at increasing rates at each drug level.

Mapping data was analyzed using custom MATLAB scripts. Data was linearly detrended and low-pass filtered with a cutoff frequency of 32 Hz. Automated filters were applied to remove excessively noisy or low-signal channels, and this was sometimes supplemented by manual removal of channels with poor signal. Activation maps were constructed using a 5-point derivative to identify the time of maximum upstroke rate of the action potential, and fit in x-y-t space to an ellipsoidal cone (Supplementary Fig. 1). Conduction velocities (CV) in the longitudinal and transverse directions were calculated as vectors (position, direction, and magnitude) starting at the vertex of the cone with magnitudes equal to the reciprocal slope of the cone along the major and minor axes, respectively. Action potential durations at 30 and 80 percent repolarization (APD_{30} and APD_{80}) were also calculated from the optical voltage signal.

2.6. Statistics

All data are presented as mean ± SD, except when stated otherwise. Anisotropy ratio and nuclear elongation were log transformed to make them more normally distributed since they were right-tailed. They were expressed as the log-transformed mean as well as the interval of the log-transformed mean plus or minus one SD, after inverse transformation back into linear space (see Supplementary Material for more details). Paired t-test was used for statistical significance between experimental groups, except when data were normalized and

then compared to control (Figs. 6D and 7C,D), in which case an unequal variance t-test was used to compare them to 1. Differences were considered statistically significant at $p < 0.05$.

3. Results

3.1. Preparation of thin decellularized slices of ECM

Slices of rat ECM were prepared by starting with Langendorff perfusion of whole rat hearts with deionized water (Fig. 1A). Ventricular tissue was excised, embedded in agarose (Fig. 1B) and sectioned into 5–8 mm-diameter, 300 μm-thick slices (Fig. 1C). Following treatment by SDS and Triton X-100, the sectioned slices became transparent (Fig. 1D). Slices of ECM were also prepared from left ventricles of pig hearts (Fig. 1E). The tissue was frozen, cut as 14 or 16 mm-diameter plugs, and a 1 cm-deep epicardial portion was cut out and embedded in agarose in a 35 mm dish (Fig. 1F). These tissue plugs were then sectioned into 300 μm-thick slices (Fig. 1G) and decellularized by SDS and Triton X-100, becoming nearly transparent (Fig. 1H). Slices of decellularized ECM did not maintain their shape when lifted out of liquid. To allow for easy handling and cell seeding, each slice was carefully spread over a plastic coverslip and hooked onto the edges of the coverslip (Fig. 1H).

Because the slices were only 300 μm-thick, they were decellularized after only 3.5 h in detergents, and then washed overnight in PBS or HBSS. Imaging of collagen using SHG showed that fiber alignment and structure was maintained after decellularization (Fig. 2A,B). Images of phalloidin staining for F-actin and DAPI counterstaining for nuclei showed cells were present in native tissue slices (Fig. 2C) and absent in decellularized slices (Fig. 2D). Cryosections of the ECM were visualized before and after decellularization using phase contrast imaging (Fig. 2E,F) and showed that the thickness of the ECM decreased from 301 ± 36 μm (n = 4) prior to decellularization to 61 ± 17 μm (n = 3) post-decellularization. DNA content decreased from 2.0 ± 0.6 (n = 8) to 0.12 ± 0.10 (n = 4) μg/mg initial dry weight, and dry weight decreased from 10.2 ± 3.5 (n = 8) to 0.9 ± 0.2 mg (n = 4). Staining for ECM components collagen I, collagen III, and laminin showed retention of these proteins and, importantly, preservation of their native structure and fiber alignment (Fig. 3). Uniaxial tensile strain testing along the longitudinal fiber direction revealed lower absolute force at a given level of strain for decellularized slices compared with native slices (Supplementary Fig. 2A), which we attribute to loss of cellular material. However, tissue stress calculated by normalizing measured force by sample thickness (which, for a decellularized slice, was approximately one-fifth of the native tissue thickness (Fig. 2E,F)), and tangential moduli at a given level of strain were higher in decellularized slices by a factor of 2.5–5. (Supplementary Fig. 2B). Further, the elastic modulus at 5% strain was approximately 69 kPa and 95 kPa for native tissue samples but approximately 109 kPa and 119 kPa for decellularized samples.

3.2. Location and orientation of cells seeded on thin slices of decellularized ECM

Freshly isolated NRVCs were seeded on ECM from both rat and pig to form EHS. ECM slices that were not tethered to coverslips compacted into a ball after cell seeding, making them unsuitable for microscopy or experimentation. EHS were imaged with calcein and

DRAQ5 for live cells and SHG for collagen so that cell location and orientation could be visualized relative to the collagen matrix in a z-stack (Fig. 4 and Supplementary Video 1). During the first 3–4 days in culture, the cells elongated from their initial rounded shape and by 5–7 days aligned along the direction of the ECM fibers (Fig. 4A). The half-maximum of the SHG signal was used to define the surface of the ECM. Three μm below the surface of the ECM, cells were still densely packed (Fig. 4A), while 30 μm below the surface some cells could still be found, but were sparse (Fig. 4B). Measurements of calcein and SHG intensity as a function of depth (Fig. 4C,D), as well as depth-coded images of calcein staining (Supplementary Fig. 3), showed that the cells were located primarily on the surface of the collagen matrix, but with some penetration into the depth.

Supplementary data related to this article can be found online at http://dx.doi.org/10.1016/j.biomaterials.2015.03.026.

Live/dead staining showed few dead cells in EHS at day 7 (Fig. 5A,E). Myocytes had well-formed sarcomeric structure (Fig. 5B,F) and expressed punctate patterns of the gap junctional protein connexin 43 (Fig. 5F). Staining with cTnI and vimentin revealed the presence of mostly myocytes and some non-myocytes (Fig. 5C,G). In general, cells were elongated and aligned (Fig. 5B,C,F,G). Elongation and alignment were quantified by the shape of the cells' nuclei, which had a mean elongation (ratio of long axis/short axis) of 2.0 (1.4–2.9) and angular standard deviation of 25° in recellularized rat ECM, and elongation of 2.1 (1.5–2.9) and angular standard deviation of 20° in recellularized pig ECM (n = 149 and 76 nuclei, respectively, Fig. 5D,H). Because pig ECM tended to produce an alignment of cells that was more globally uniform than that in rat ECM, the majority of the following functional studies were carried out on EHS made from pig ECM.

3.3. Contraction of EHS

During culture, the beating rate of some EHS made with pig ECM was recorded daily. Two days after cell plating, approximately 40% of the EHS exhibited small asynchronous areas of contraction, 40% showed coordinated contraction across a 0.55 mm^2 field of view, and 20% were quiescent. Over the next 4 days, the fraction of EHS with asynchronous contraction decreased to zero, while the fraction of quiescent EHS increased. By 7 days, about 60% of the EHS were quiescent, while the remainder contracted synchronously and intermittently. Almost all of the EHS that were electrically stimulated on days 7–8 after characterization of spontaneous beating exhibited either synchronous contraction across the EHS if assayed for contractility (Supplementary Video 2), or activation across the entire EHS if optically mapped (Supplementary Video 4), demonstrating that EHS quiescence was not due to cell death. To quantitate contraction, one corner of an EHS was unhooked from the coverslip so that shortening could be observed during electrical pacing (Fig. 6A–C and Supplementary Video 3). Using displacement as a surrogate for contractile force, we measured the force-frequency relationship of the EHS, and found a statistically significant decrease in contractile force at pacing rates of 4 and 5 Hz relative to 2 Hz (Fig. 6D, n = 4–6 EHS).

3.4. Anisotropic electrical conduction, response to lidocaine, and reentrant activity in EHS

EHS made from rat ECM were field stimulated at different pacing rates, and optical mapping demonstrated action potential propagation over nearly the entire tissue when field stimulation was slightly suprathreshold (Fig. 7A,B). EHS made from pig ECM were stimulated at their center by a point electrode. Optical maps enabled the characterization of action potential propagation and morphology (Fig. 7C,D and Supplementary Video 4). At 2 Hz, EHS (n = 17) had a normal action potential profile with an APD_{80} of 157 ± 39 ms, similar to that reported in NRVC monolayers (137 ± 13 ms on day 6) [12], and an APD_{30} of 69 ± 15 ms. Longitudinal CV was 14.4 ± 5.5 cm/s, transverse CV was 7.5 ± 3.4 cm/s, and the anisotropy ratio of conduction velocities (AR) was 2.0 (1.4–2.8). For pacing rates increasing from 1 to 5 Hz, action potential duration (Fig. 7E) and conduction velocities in the longitudinal and transverse directions (Fig. 7F) all had negative rate-dependencies, while AR remained approximately constant at 2.0. Some EHS were kept in culture for 21 days and could be paced and optically mapped (Supplementary Fig. 4). Adding increasing doses of lidocaine to EHS (n = 4–5) resulted in a statistically significant dose-dependent decrease in conduction velocity (Fig. 8A–C) and maximum capture rate (Fig. 8D) that was largely reversed after washout. Fractional conduction slowing was more pronounced in the longitudinal than transverse direction (Fig. 8A–C).

Reentrant activity could be induced in EHS by pacing at progressively faster rates. At slow pacing rates, EHS exhibited approximately elliptical wavefronts spreading from a point stimulus (Fig. 9A), but as pacing rates increased, a reentrant spiral wave sometimes formed (Fig. 9B–G,K), which could be terminated by a high-intensity electrical field pulse (Fig. 9H–K and Supplementary Video 5). In 17 EHS that were rapidly paced, 8 had one or more pace-inducible spiral waves, which were induced at a pacing rate of 6.3 ± 1.4 Hz. All of the spiral waves could be terminated by field stimulation of 6–24 V/cm.

Supplementary data related to this article can be found online at http://dx.doi.org/10.1016/j.biomaterials.2015.03.026.

4. Discussion

Since the seminal work by Ott et al. demonstrating the decellularization and subsequent repopulation of a rat heart [4], the use of decellularized native tissues as natural scaffolds for engineered organs and tissues has become widely investigated [13]. A common method to decellularize cardiac tissue is perfusion of the whole organ with detergents and/or enzymes, and has been successfully applied to rat [4,8,14,10], pig [5], and mouse [9] hearts. However, recellularization of the decellularized heart, either through the coronary circulation or by direct injection, has not succeeded in repopulating the tissue evenly. The study of recellularized hearts has focused primarily on mechanical function, with only two electrophysiological reports to date. Those reports used calcium indicator dyes in hearts recellularized by coronary perfusion. In one, electrical activity was shown to propagate over a 150 μm square area of a recellularized mouse ventricle [9], while in the other, cells in recellularized rat ventricles formed patches that were either well synchronized, unsynchronized but organized, or disorganized [10].

Alternatively, global recellularization of isolated slices of myocardium is a much simpler proposition because cells can be seeded directly onto the exposed surface, although penetration of cells into the interior is limited. Two to 10 mm-thick slices of dissected porcine heart have been decellularized by mechanical agitation [6], sonication [15], or perfusion through a blood vessel [16], but these procedures used long treatment times (10 days, 2.5 weeks, and 5 days, respectively), which run the risk of excessive degradation of constituents of the ECM [17].

Our strategy is to plate cardiomyocytes onto very thin sections of decellularized ECM. By cutting the tissue chunks into 300 μm-thick sections (Fig. 1), decellularization time by orbital agitation is greatly reduced to around 3.5 h. Godier-Furnemont et al. [18] and Oberwallner et al. [7] also used orbital agitation to decellularize 300 μm-thick slices obtained from human heart, but over a period of 8 h and 1 week, respectively. Following decellularization, our ECM slices thin down to around 60 μm (Fig. 2F), but can still be handled manually. By using tissue plugs from porcine hearts, we can obtain 10–20 sections per plug. Cells can be directly plated on top of the ECM, and the recellularized tissue is more homogeneous than that made by perfusion recellularization of whole hearts. Other advantages of this approach are that EHS are relatively transparent and can be easily monitored during culture using bright-field microscopy and that cell shape, orientation, density and connectivity can be visualized more easily than when the cells are fully embedded in a 3-D tissue matrix.

4.1. Myocytes in EHS experience important physiological cues from 3-D matrix

Fully 3-D engineered cardiac tissues have been achieved by culturing myocytes in hydrogels or on synthetic scaffolds [2]. This approach has the advantage of control of the scaffold composition and shape, and has been successfully utilized to produce physiologically functional cardiac tissue constructs [2]. Uniformity of cell density and connectivity through the depth of the tissue remains a challenge, although recent advances appear to have largely addressed this problem for certain types of constructs [1]. However, these systems lack many of the instructive cues offered by the ECM [19].

Following decellularization, the thickness of the sliced ECM reduces from 300 μm to around 60 μm (Fig. 2E,F). Similarly, Ott, et al. [4] also found a significant decrease in thickness (from an average of 3.59 to 0.24 mm) after perfusion decellularization of whole hearts. We found that cells in EHS lie mostly at the surface of the slice and experience important biochemical, structural, and mechanical signals from the underlying 3-D ECM, a situation referred to as “2.5-D” [20]. If left untethered, the EHS would compact and ball up, making them unsuitable for further experimentation. However, attachment of the decellularized slices to coverslips (Fig. 1H) maintains the distance between ECM fibers in the x-y plane. Cells can settle into small openings and valleys of the ECM matrix, and may extend to a limited degree into the matrix (Fig. 4).

Native ECM contains a complex mixture of structural proteins that interact with the myocytes and influence their adhesion, growth, and contractile function [19]. For example, the ECM can retain growth factors and mediate the availability of these and other signaling molecules [21]. Additionally, cell function is affected by integrin-matrix binding and other

biomechanical pathways [21,22]. Although the degree of retention of different ECM constituents varies with the decellularization method [14], the complex protein composition of native ECM is largely retained following decellularization, which is an advantage over scaffolds that provide only one or a small number of ECM proteins, since cell growth depends on a variety of ECM proteins [8,23].

The growth of cultured myocytes also depends on the stiffness of the substrate, and appears to be best when the tangential modulus is close to physiological values [24]. Our measurements of the tangential modulus of decellularized slices show values only 2.5–5 fold higher than that of native matrix (Supplementary Fig. 2). The elastic moduli we calculated for 5% strain (69 kPa and 95 kPa for native samples along with 109 kPa and 119 kPa for decellularized samples) were within an order of magnitude of those previously reported for animal [25] and human [26] hearts, which range from 18 kPa to 30 kPa. Importantly, the ECM is sufficiently compliant to be substantially deformed by cell contraction (Fig. 6).

A special advantage of native ECM is that it is a natural scaffold that contains a fine collagen weave that is aligned along the myocardial cells. This alignment is retained following decellularization (Figs. 2A,B–4) [4,7]. Because structural cues on the micro- and nano-scale are sufficient to cause myocyte alignment [27], the ECM promotes alignment of the engrafted cardiomyocytes.

Thus, important physiological cues that have beneficial effects on myocyte function are still present in EHS. Indeed, we found that NRVCs in our EHS remained electrically connected and active for at least 21 days in culture, a period of time that is much longer than in NRVC monolayers, which have a maximal culture period of about ten days in our lab [28]. Additionally, Oberwallner and co-workers seeded neonatal mouse cardiomyocytes or induced pluripotent stem cell-derived cardiomyocytes onto 300 μm-thick slices obtained from decellularized human heart, and reported cell attachment and survival, visible contraction of the matrix, and increased cellular metabolic activity compared with cells cultured on tissue culture plastic [7].

4.2. Myocytes are elongated and aligned in EHS

In native atrial and ventricular myocardium, cardiac cells have an elongated rod shape and are aligned along fiber directions, which is important for efficient force production. When cardiomyocytes are cultured on chemically or topologically defined anisotropic substrates, they have an elongated shape and align along a preferred direction, with better ultrastructural organization and higher contractile force than when cultured on uniform surfaces [29]. Cell elongation and alignment have also been shown to affect the intracellular handling of calcium [29,30], which is vital to excitation-contraction coupling in the heart and, when disturbed, is a mechanism for many cardiac arrhythmias [31]. We measured nuclear elongation as a surrogate for cellular elongation because nuclear deformation parallels cellular deformation and anisotropy [32], and because the functional consequences of cell shape are mediated by changes in gene expression arising from deformation of the nucleus by microtubules and intermediate filaments and subsequent mechanotransduction events [33].

Another important functional consequence of cell elongation and alignment is anisotropic action potential propagation [34], a property of native tissue which, under pathological conditions, can cause propagation to locally fail and create arrhythmic, reentrant circuits [35]. Fiber alignment and anisotropy can vary with location in the heart, and while sophisticated microprinting techniques can be used to recapitulate a DT-MRI image as a two-dimensional pattern of cells [36], our approach is to use the ECM as a template for cellular patterning. EHS can be prepared from any region of the heart to study the effects of the local structure. For example, cells grown on the endocardial surface of decellularized hearts do not align [5], while cells in our slices, taken from near the epicardium, do. To our knowledge, our study is the first demonstration of anisotropic conduction of electrical activity in recellularized ECM. In EHS, the fibrillar structure of the ECM (Figs. 2B and 3) leads to cell elongation and alignment (Figs. 4 and 5), which then results in anisotropic conduction (Figs. 7C,F, 8 and 9). AR is around 2.0, which falls within the range of 1.4–3.7 that can be achieved with NRVC monolayers cultured on anisotropic 2-D substrates [37] but is somewhat lower than the AR of ~2.7 found in adult ventricular muscle [38].

4.3. Myocytes in EHS are mechanically active and contract synchronously

Myocytes in EHS form a confluent, contractile, syncytium (Figs. 4–6, Supplementary Fig. 3) that is electrically coupled by gap junctions (Fig. 5F). The myocytes produce enough force to overcome the stiffness of the ECM, resulting in EHS shortening during contraction (Fig. 6, Supplementary Video 2). Optical mapping showed that during spontaneous activity or electrical pacing, action potentials propagate through the entire surface of the EHS (Fig. 7A,C), which act to initiate and synchronize contraction throughout the EHS. Measurements of the force-frequency relation (Fig. 6D) show a monotonic decrease in contraction from 1 to 5 Hz pacing rate, consistent with measurements in other NRVC-based engineered cardiac tissues [39] and native rat myocardium [40].

4.4. EHS exhibit physiological response to lidocaine

The fact that EHS form an anisotropic syncytium allowed us to study the effect of drugs on longitudinal and transverse conduction velocities, which is not possible in simpler systems. To demonstrate this, we applied increasing doses of lidocaine, a sodium channel blocker that is clinically used as an antiarrhythmic agent [41], and measured its effect on conduction velocity and maximum capture rate. We found a 19% and 14% decrease in CV at 2 Hz by 90 μM lidocaine in the longitudinal and transverse directions, respectively (Fig. 8C), which is similar to the reported ~19% increase in conduction time at 1 Hz by 100 μM lidocaine in Langendorff-perfused rabbit hearts [42], although direct comparison of these values is complicated by the different models and pacing rates. Additionally, we found more fractional slowing in the longitudinal direction (Fig. 8C) which is consistent with findings in Langendorff-perfused dog hearts [43]. We also found a dose-dependent decrease in maximum capture rate by lidocaine (Fig. 8D), which is expected due to its sodium channel blocking activity [41]. These findings demonstrate the applicability of EHS to studying drug effects on cardiac tissue.

4.5. Potential applications of EHS

EHS are an attractive model for physiological and pathophysiological studies because of their contractile and electrophysiological function at a tissue level. Their macroscopic 2.5-dimensional nature represents a step up in structural and functional complexity from one-dimensional tissue constructs (strips, strands, fiber bundles), opening the door to studies involving biaxial stretch or two-dimensional tissue electrophysiology. EHS can be maintained in culture for at least 21 days (Supplementary Fig. 4), raising the possibility of their use for long-term drug studies. The ECM scaffold is an aligned substrate that is inexpensive and does not require specialized facilities to produce. Although we used NRVCs as the cardiac cell type, other cell types, such as cardiomyocytes derived from human embryonic stem cells or induced pluripotent stem cells, can be substituted, and this is the subject of an ongoing study by our group.

Although other investigators have recellularized whole-heart ECM with cardiomyocytes, the distribution of cells is generally patchy and not well-coupled electrically, making them prone to arrhythmia [10]. In EHS, myocytes are electrophysiologically active throughout, behave as an electrically coupled syncytium, and exhibit contraction and anisotropic conduction similar to that in native tissue, with physiological (for rat) negative rate-dependencies of contractility (Fig. 6D), action potential duration (Fig. 7E), conduction velocity (Fig. 7F), as well as physiological drug response (Fig. 8). Unlike single cells or 1-D tissue constructs, EHS allow 2-D wave propagation and are large enough in area to support reentrant arrhythmias (Fig. 9), which are the more life-threatening forms of arrhythmia (like fibrillation). Cell monolayers also support reentrant arrhythmias and have been used for mechanistic studies [44], but they are cultured in a less physiological microenvironment consisting of a rigid flat surface typically coated with a single ECM protein.

EHS may also prove to be valuable for studies of myocardial contraction. With the proper interface, they can be stretched to different resting lengths. By changing the thickness of the EHS, the mechanical load presented to the cells can be varied [45,46]. Additionally, EHS may be superior to adherent cells or cell monolayers for metabolic studies, because of their ability to perform mechanical work.

EHS will undoubtedly be useful for a better understanding of the physiological and pathophysiological roles of the ECM. For example, they can be formed using decellularized slices from different regions of the heart, from old vs. young hearts, and from healthy vs. diseased hearts, all of which can have differing compositions and structure of ECM [8,47,48]. By obtaining sequential ECM slices from the same tissue plug, our approach readily yields multiple EHS with similar characteristics, making them effective as a tool for *in vitro* investigations.

Finally, in terms of clinical applications, EHS may be an attractive alternative to the method of forming myocardial patches by stacking individual sheets of myocytes grown on flat surfaces [49]. EHS may also be useful as a preclinical model for drug testing, much as native cardiac slices are being used [50]. However, functional variability between EHS remains a present limitation for this use, and improved protocols for their production may be needed.

5. Conclusion

Engineered heart slices are essentially 2.5-dimensional tissues that retain important biochemical, structural and mechanical aspects of the extracellular matrix. Cardiomyocytes grown in EHS are aligned and can be maintained in culture, resulting in a tissue that has anisotropic properties similar to native tissue. EHS contract synchronously throughout and are electrophysiologically active, behaving as an integrated, functional tissue. Thus, they can serve as a model system for studies of physiological and pathophysiological myocardial function “in a dish.”

Supplementary Material

Refer to Web version on PubMed Central for supplementary material.

Acknowledgments

This work was supported by Maryland Stem Cell Research Fund grant 2013-MSCRF–II–0045 (L.T.) and NIH grant S10 RR025544 (L.T.) as well as Mid-Atlantic AHA predoctoral fellowships (A.B. and G.M.K).We thank Dr. Gordon Tomaselli for the use of his Nanodrop spectrophotometer and Esther Kieserman for microscopy assistance. The multiphoton microscope used for SHG imaging was funded by NIH Grant S10 RR024550 (Scot Kuo, PI).

References

1. Hirt MN, Hansen A, Eschenhagen T. Cardiac tissue engineering: state of the art. Circ Res. 2014; 114:354–367. [PubMed: 24436431]
2. Eschenhagen T, Eder A, Vollert I, Hansen A. Physiological aspects of cardiac tissue engineering. Am J Physiol Heart Circ Physiol. 2012; 303:H133–H143. [PubMed: 22582087]
3. Vunjak-Novakovic G, Eschenhagen T, Mummery C. Myocardial tissue engineering: in vitro models. Cold Spring Harb Perspect Med. 2014; 4
4. Ott HC, Matthiesen TS, Goh S-K, Black LD, Kren SM, Netoff TI, et al. Perfusion-decellularized matrix: using nature's platform to engineer a bioartificial heart. Nat Med. 2008; 14:213–221. [PubMed: 18193059]
5. Wainwright JM, Czajka Ca, Patel UB, Freytes DO, Tobita K, Gilbert TW, et al. Preparation of cardiac extracellular matrix from an intact porcine heart. Tissue Eng Part C Methods. 2010; 16:525–532. [PubMed: 19702513]
6. Eitan Y, Sarig U, Dahan N, Machluf M. Acellular cardiac extracellular matrix as a scaffold for tissue engineering: in vitro cell support, remodeling, and biocompatibility. Tissue Eng Part C Methods. 2010; 16:671–683. [PubMed: 19780649]
7. Oberwallner B, Brodarac A, Choi Y-H, Saric T, Anić P, Morawietz L, et al. Preparation of cardiac extracellular matrix scaffolds by decellularization of human myocardium. J Biomed Mater Res Part A. 2013; 102:3263–3272.
8. Williams C, Quinn KP, Georgakoudi I, Black LD. Young developmental age cardiac extracellular matrix promotes the expansion of neonatal cardiomyocytes in vitro. Acta Biomater. 2014; 10:194–204. [PubMed: 24012606]
9. Lu T-Y, Lin B, Kim J, Sullivan M, Tobita K, Salama G, et al. Repopulation of decellularized mouse heart with human induced pluripotent stem cell-derived cardiovascular progenitor cells. Nat Commun. 2013; 4:2307. [PubMed: 23942048]
10. Yasui H, Lee J-K, Yoshida A, Yokoyama T, Nakanishi H, Miwa K, et al. Excitation propagation in three-dimensional engineered hearts using decellularized extracellular matrix. Biomaterials. 2014; 35:7839–7850. [PubMed: 24952982]
11. Lim ZY, Maskara B, Aguel F, Emokpae R, Tung L. Spiral wave attachment to millimeter-sized obstacles. Circulation. 2006; 114:2113–2121. [PubMed: 17088465]

12. Sathaye A, Bursac N, Sheehy S, Tung L. Electrical pacing counteracts intrinsic shortening of action potential duration of neonatal rat ventricular cells in culture. J Mol Cell Cardiol. 2006; 41:633–641. [PubMed: 16950369]
13. Tapias LF, Ott HC. Decellularized scaffolds as a platform for bioengineered organs. Curr Opin Organ Transpl. 2014; 19:145–152.
14. Akhyari P, Aubin H, Gwanmesia P, Barth M, Hoffmann S, Huelsmann J, et al. The quest for an optimized protocol for whole-heart decellularization: a comparison of three popular and a novel decellularization technique and their diverse effects on crucial extracellular matrix qualities. Tissue Eng Part C Methods. 2011; 17
15. Wang B, Borazjani A, Tahai M, Curry ALDJ, Simionescu DT, Guan J, et al. Fabrication of cardiac patch with decellularized porcine myocardial scaffold and bone marrow mononuclear cells. J Biomed Mater Res A. 2010; 94:1100–1110. [PubMed: 20694977]
16. Sarig U, Au-yeung GCT, Wang Y, Bronshtein T, Dahan N, Boey FYC, et al. Thick acellular heart extracellular matrix with inherent vasculature: a potential platform for myocardial tissue regeneration. Tissue Eng Part A. 2012; 18:2125–2137. [PubMed: 22663095]
17. Crapo PM, Gilbert TW, Badylak SF. An overview of tissue and whole organ decellularization processes. Biomaterials. 2011; 32:3233–3243. [PubMed: 21296410]
18. Godier-Furnémont AFG, Martens TP, Koeckert MS, Wan L, Parks J, Arai K, et al. Composite scaffold provides a cell delivery platform for cardiovascular repair. Proc Natl Acad Sci U S A. 2011; 108:7974–7979. [PubMed: 21508321]
19. Bowers SLK, Banerjee I, Baudino TA. The extracellular matrix: at the center of it all. J Mol Cell Cardiol. 2010; 48:474–482. [PubMed: 19729019]
20. Prestwich GD. Simplifying the extracellular matrix for 3-D cell culture and tissue engineering: a pragmatic approach. J Cell Biochem. 2007; 101:1370–1383. [PubMed: 17492655]
21. Fan D, Creemers EE, Kassiri Z. Matrix as an interstitial transport system. Circ Res. 2014; 114:889–902. [PubMed: 24577968]
22. McCain ML, Parker KK. Mechanotransduction: the role of mechanical stress, myocyte shape, and cytoskeletal architecture on cardiac function. Pflugers Arch. 2011; 462:89–104. [PubMed: 21499986]
23. LaNasa SM, Bryant SJ. Influence of ECM proteins and their analogs on cells cultured on 2-D hydrogels for cardiac muscle tissue engineering. Acta Biomater. 2009; 5:2929–2938. [PubMed: 19457460]
24. Jacot JG, McCulloch AD, Omens JH. Substrate stiffness affects the functional maturation of neonatal rat ventricular myocytes. Biophys J. 2008; 95:3479–3487. [PubMed: 18586852]
25. Berry JM, Naseem RH, Rothermel BA, Hill JA. Models of cardiac hypertrophy and transition to heart failure. Drug Discov Today Dis Model. 2007; 4:197–206.
26. Couade M, Pernot M, Messas E, Bel A, Ba M, Hagege A, et al. Vivo quantitative mapping of myocardial stiffening and transmural anisotropy during the cardiac cycle. IEEE Trans Med Imaging. 2011; 30:295–305. [PubMed: 20851788]
27. Kim D-H, Lipke Ea, Kim P, Cheong R, Thompson S, Delannoy M, et al. Nanoscale cues regulate the structure and function of macroscopic cardiac tissue constructs. Proc Natl Acad Sci U S A. 2010; 107:565–570. [PubMed: 20018748]
28. Sekar RB, Kizana E, Smith RR, Barth AS, Zhang Y, Marbán E, et al. Lentiviral vector-mediated expression of GFP or Kir2.1 alters the electrophysiology of neonatal rat ventricular myocytes without inducing cytotoxicity. Am J Physiol Heart Circ Physiol. 2007; 293:H2757–H2770. [PubMed: 17675572]
29. Kuo P-L, Lee H, Bray M-A, Geisse NA, Huang Y-T, Adams WJ, et al. Myocyte shape regulates lateral registry of sarcomeres and contractility. Am J Pathol. 2012; 181:2030–2037. [PubMed: 23159216]
30. Chung C-Y, Bien H, Entcheva E. The role of cardiac tissue alignment in modulating electrical function. J Cardiovasc Electrophysiol. 2007; 18:1323–1329. [PubMed: 17916158]
31. Weiss JN, Karma A, Shiferaw Y, Chen P-S, Garfinkel A, Qu Z. From pulsus to pulseless: the saga of cardiac alternans. Circ Res. 2006; 98:1244–1253. [PubMed: 16728670]

32. Bray M-AP, Adams WJ, Geisse NA, Feinberg AW, Sheehy SP, Parker KK. Nuclear morphology and deformation in engineered cardiac myocytes and tissues. Biomaterials. 2010; 31:5143–5150. [PubMed: 20382423]
33. Dalby MJ. Topographically induced direct cell mechanotransduction. Med Eng Phys. 2005; 27:730–742. [PubMed: 15921949]
34. Spach MS, Heidlage JF, Barr RC, Dolber PC. Cell size and communication: role in structural and electrical development and remodeling of the heart. Heart Rhythm. 2004; 1:500–515. [PubMed: 15851207]
35. Spach MS, Dolber PC. Relating extracellular potentials and their derivatives to anisotropic propagation at a microscopic level in human cardiac muscle. Evidence for electrical uncoupling of side-to-side fiber connections with increasing age. Circ Res. 1986; 58:356–371. [PubMed: 3719925]
36. Bian W, Jackman CP, Bursac N. Controlling the structural and functional anisotropy of engineered cardiac tissues. Biofabrication. 2014; 6:024109. [PubMed: 24717534]
37. Bursac N, Parker KK, Iravanian S, Tung L. Cardiomyocyte cultures with controlled macroscopic anisotropy: a model for functional electrophysiological studies of cardiac muscle. Circ Res. 2002; 91:45e–54e.
38. Kleber A, Janse M, Fast V. Normal and abnormal conduction in the heart. Handb Physiol Cardiovasc Syst Hear. 2002:455–530.
39. Bursac N, Kirkton RD, McSpadden LC, Liau B. Characterizing functional stem cell-cardiomyocyte interactions. Regen Med. 2010; 5:87–105. [PubMed: 20017697]
40. Schouten VJA, ter Keurs HEDJ. The force-frequency relationship in rat myocardium. Pflügers Arch. 1986; 407:14–17. [PubMed: 3737379]
41. Moreno JD, Zhu ZI, Yang P-C, Bankston JR, Jeng M-T, Kang C, et al. A computational model to predict the effects of class I anti-arrhythmic drugs on ventricular rhythms. Sci Transl Med. 2011; 3:98ra83.
42. Lu HR, Rohrbacher J, Vlaminckx E, Van Ammel K, Yan GX, Gallacher DJ. Predicting drug-induced slowing of conduction and pro-arrhythmia: identifying the “bad” sodium current blockers. Br J Pharmacol. 2010; 160:60–76. [PubMed: 20331615]
43. Anderson KP, Walker R, Lux RL, Ershler PR, Menlove R, Williams MR, et al. Conduction velocity depression and drug-induced ventricular tachyarrhythmias. Effects of lidocaine in the intact canine heart. Circulation. 1990; 81:1024–1038. [PubMed: 2155070]
44. Tung L, Zhang Y. Optical imaging of arrhythmias in tissue culture. J Electrocardiol. 2006; 39:S2–S6. [PubMed: 17015066]
45. Feng CH, Cheng YC, Chao PHG. The influence and interactions of substrate thickness, organization and dimensionality on cell morphology and migration. Acta Biomater. 2013; 9:5502–5510. [PubMed: 23201017]
46. Leong WS, Tay CY, Yu H, Li A, Wu SC, Duc DH, et al. Thickness sensing of hMSCs on collagen gel directs stem cell fate. Biochem Biophys Res Commun. 2010; 401:287–292. [PubMed: 20851103]
47. Herpel E, Singer S, Flechtenmacher C, Pritsch M, Sack F-U, Hagl S, et al. Extracellular matrix proteins and matrix metalloproteinases differ between various right and left ventricular sites in end-stage cardiomyopathies. Virchows Arch. 2005; 446:369–378. [PubMed: 15806380]
48. Sullivan KE, Quinn KP, Tang KM, Georgakoudi I, Black LD. Extracellular matrix remodeling following myocardial infarction influences the therapeutic potential of mesenchymal stem cells. Stem Cell Res Ther. 2014; 5
49. Matsuura K, Masuda S, Shimizu T. Cell sheet-based cardiac tissue engineering. Anat Rec Hob. 2014; 297:65–72.
50. Meyer T, Stuerz K, Guenther E, Edamura M, Kraushaar U. Cardiac slices as a predictive tool for arrhythmogenic potential of drugs and chemicals. Expert Opin Drug Metab Toxicol. 2010; 6:1461–1475. [PubMed: 21067457]

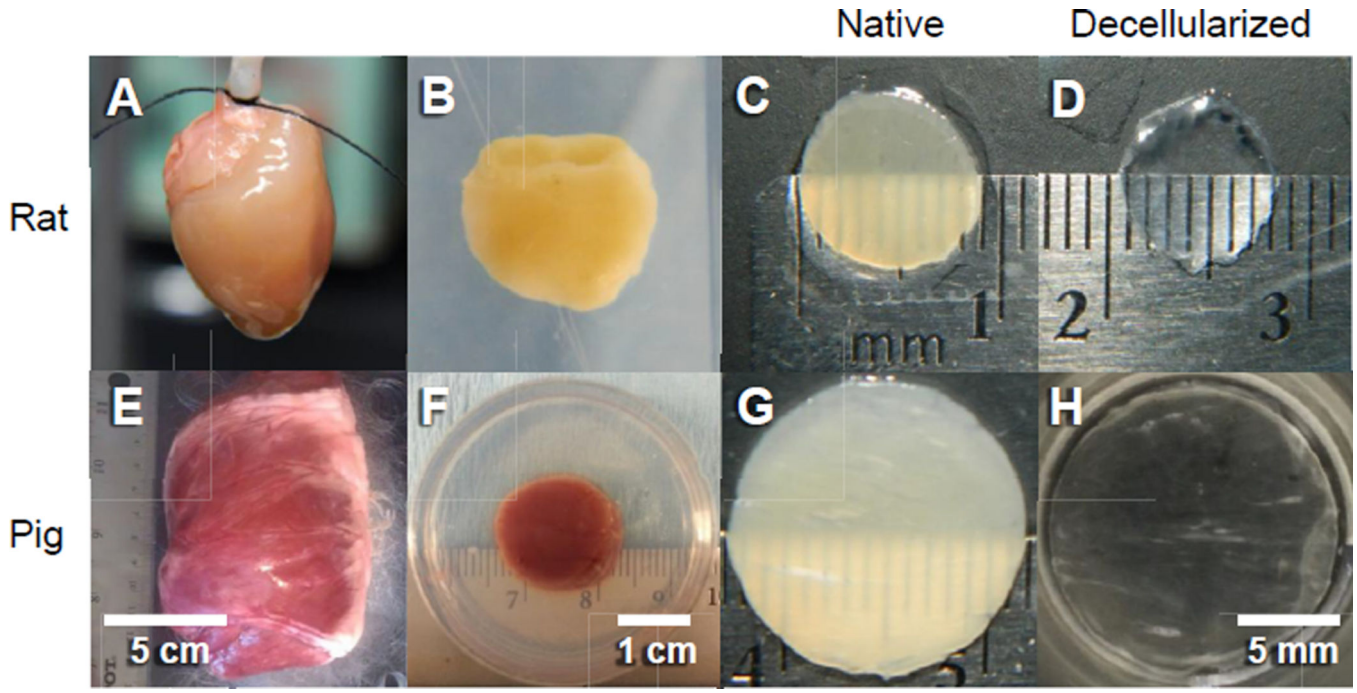

Fig. 1.

Preparation of EHS from rat and pig ECM. To make slices of rat ECM, adult rat hearts were suspended on a Langendorff perfusion setup and rinsed with filtered deionized water to remove blood and assist in cell lysis via osmotic pressure (A). After removal of the atria, the ventricles were embedded in agarose (B) for sectioning. To make slices of pig ECM, left ventricles were excised from pig hearts (E). A 1 cm-thick epicardial plug was punched out and embedded in agarose (F). Tissue from both preparations was sectioned into 300 μm-thick slices using a vibratome (C and G). Slices are shown following decellularization by SDS and Triton X-100 (D and H). H shows a slice after it was spread on a 14 mm-diameter coverslip. C, D, G, and H have the same scale.

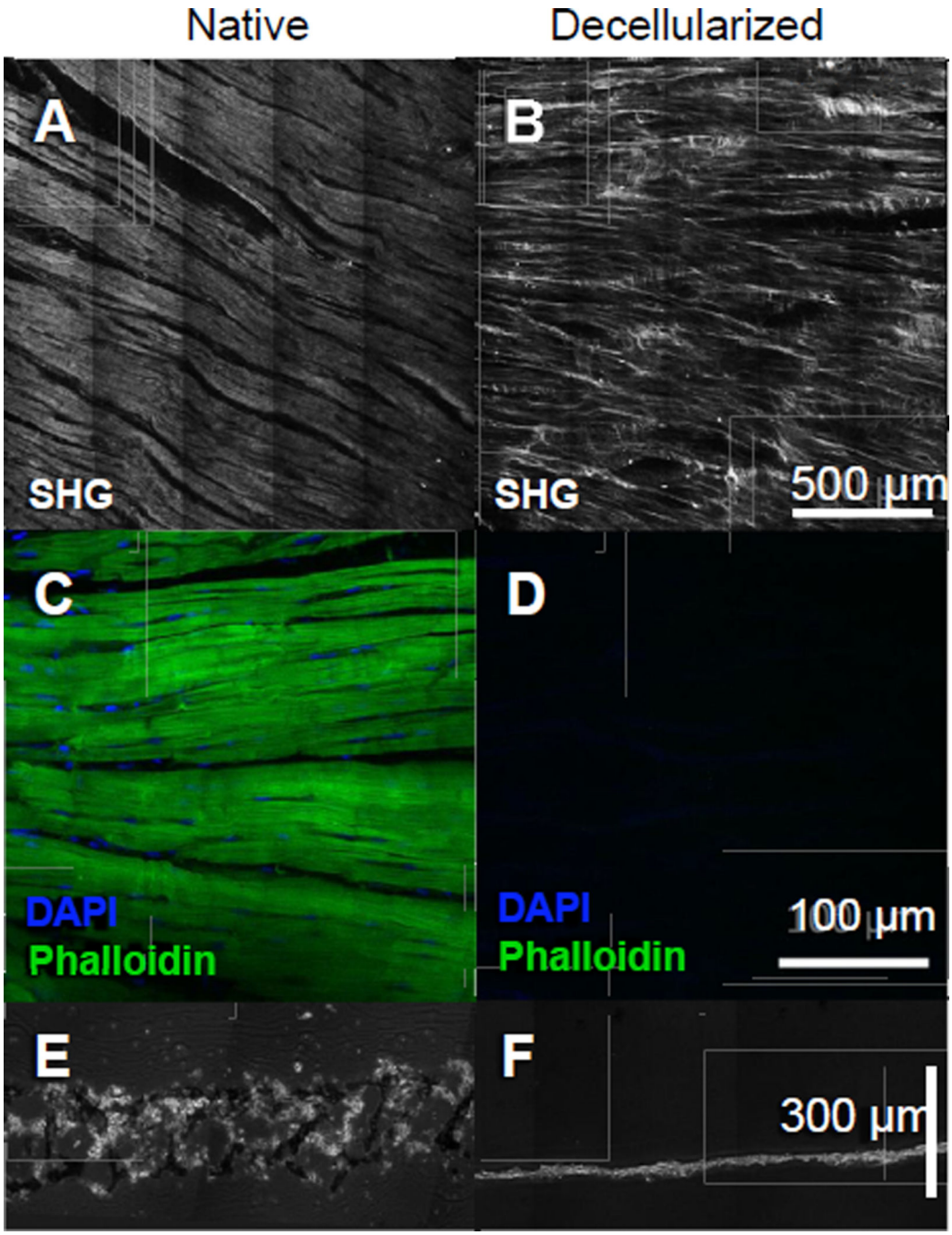

Fig. 2.

Characterization of decellularized slices of pig ECM. Second harmonic generation imaging showed similar collagen structure and alignment before (A), and after (B), decellularization. A and B have the same scale. Confocal images of native (C) and decellularized (D) pig ECM stained for nuclei (DAPI) and F-actin (phalloidin) showed a virtual absence of cellular material after decellularization. C and D have the same scale and imaging settings. Ten μm-thick cross-sections of slices of pig ECM before and after decellularization are shown using phase contrast microscopy (E and F, respectively). E and F have the same scale.

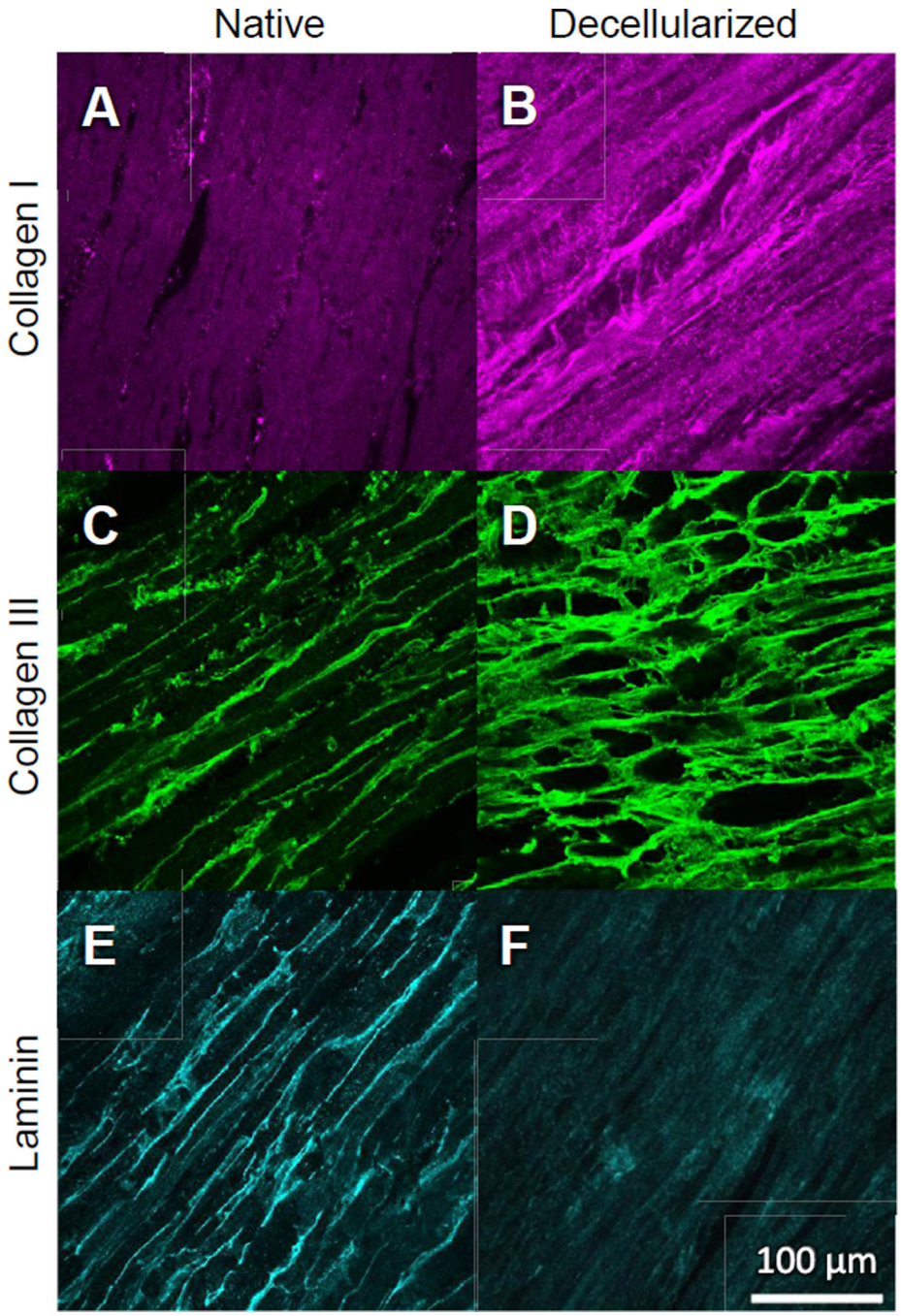

Fig. 3.

Characterization of decellularized pig ECM proteins. Immunostaining showed retention of collagen I (A–B), collagen III (C–D), and laminin (E–F), after decellularization. All panels have the same scale. Native and decellularized images in each row were acquired using the same settings.

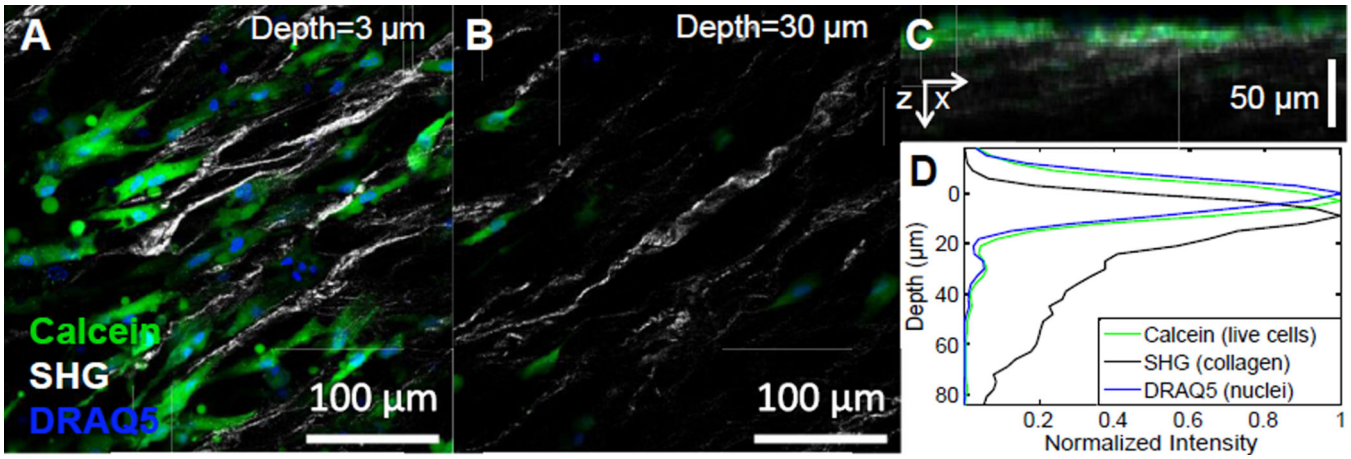

Fig. 4.

Survival and location of cells in EHS made from pig ECM. Calcein-AM (live cells), second-harmonic generation (SHG), and DRAQ5 (nuclei) were imaged 7 days after plating to create a z-stack of confocal images. A and B show x–y (en face) images from different depths, with zero depth defined to be at the half maximum of the rising edge of the SHG signal (see D). The intensity of calcein-AM, SHG, and DRAQ5 were averaged in the y-direction and plotted in the x-z plane (C). These intensities were then averaged in the x-direction and plotted as a function of z (D, normalized to maximum for each channel), and show a layer of cells residing mostly on top of the ECM. Supplementary Video 1 shows a 3-D rendering of the z-stack.

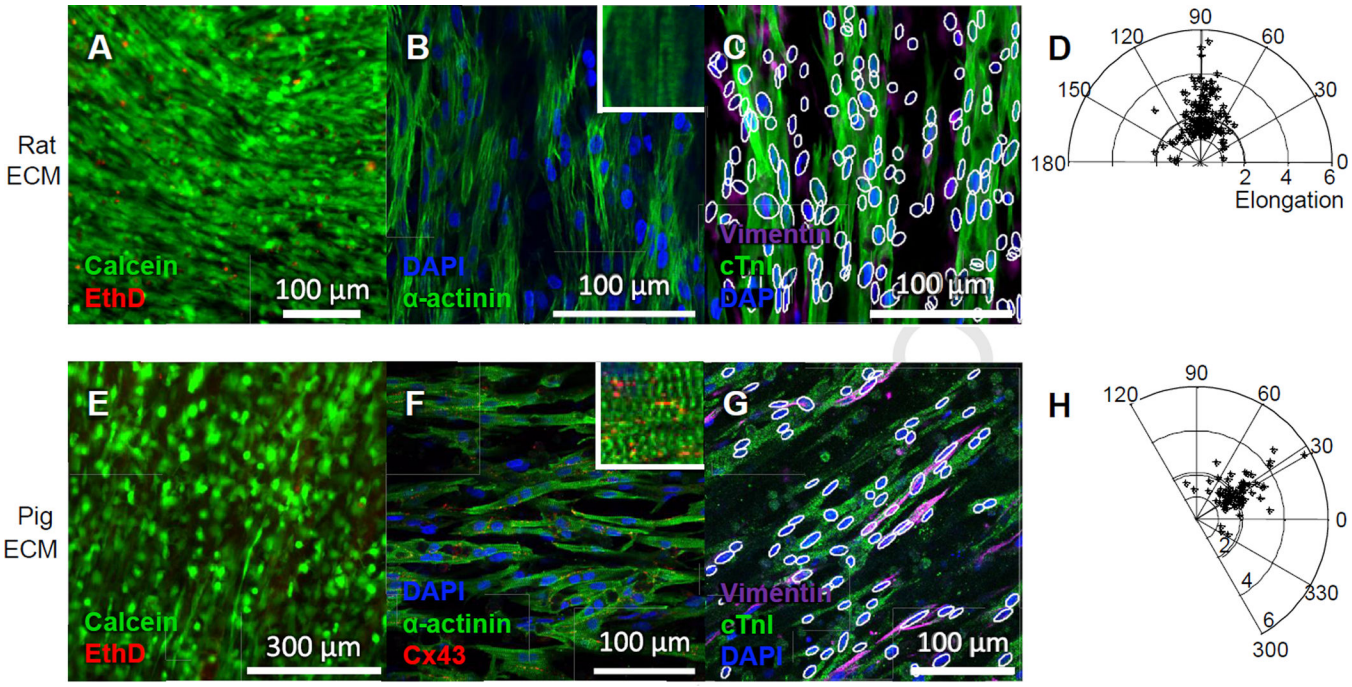

Fig. 5.

Characterization of cells in EHS made from rat and pig ECM. Staining of live cells with calcein-AM (green) and dead cells with ethidium homodimer-1 (EthD, red) reveals few dead cells in the EHS 7 days after plating (A,E). α-actinin staining (green) shows alignment and elongation of cells (B,F), and distinct sarcomeric striations (insets show portions of the images at 10 times magnification). Connexin 43 (Cx43, red) staining suggests cells are electrically coupled (F). Staining with vimentin (violet) for non-myocytes, α-actinin (green) for cardiomyocytes, and DAPI (blue) for nuclei showed mostly myocytes and some non-myocytes in EHS made from both types of ECM (C, G). Automated analysis of nuclear shapes showed they were elongated and aligned (C,D,G,H). White ellipses in C and G show fits of nuclei. Radial distances in D and H show elongation (long axis/short axis) of nuclei in C and G, respectively, while the angles show the orientation of the long axes of the nuclei. The mean orientation and elongation are marked by solid radial and circumferential lines, respectively. EHS in B,C,F,G were fixed 5–8 days after plating. (For interpretation of the references to color in this figure caption, the reader is referred to the web version of this article.)

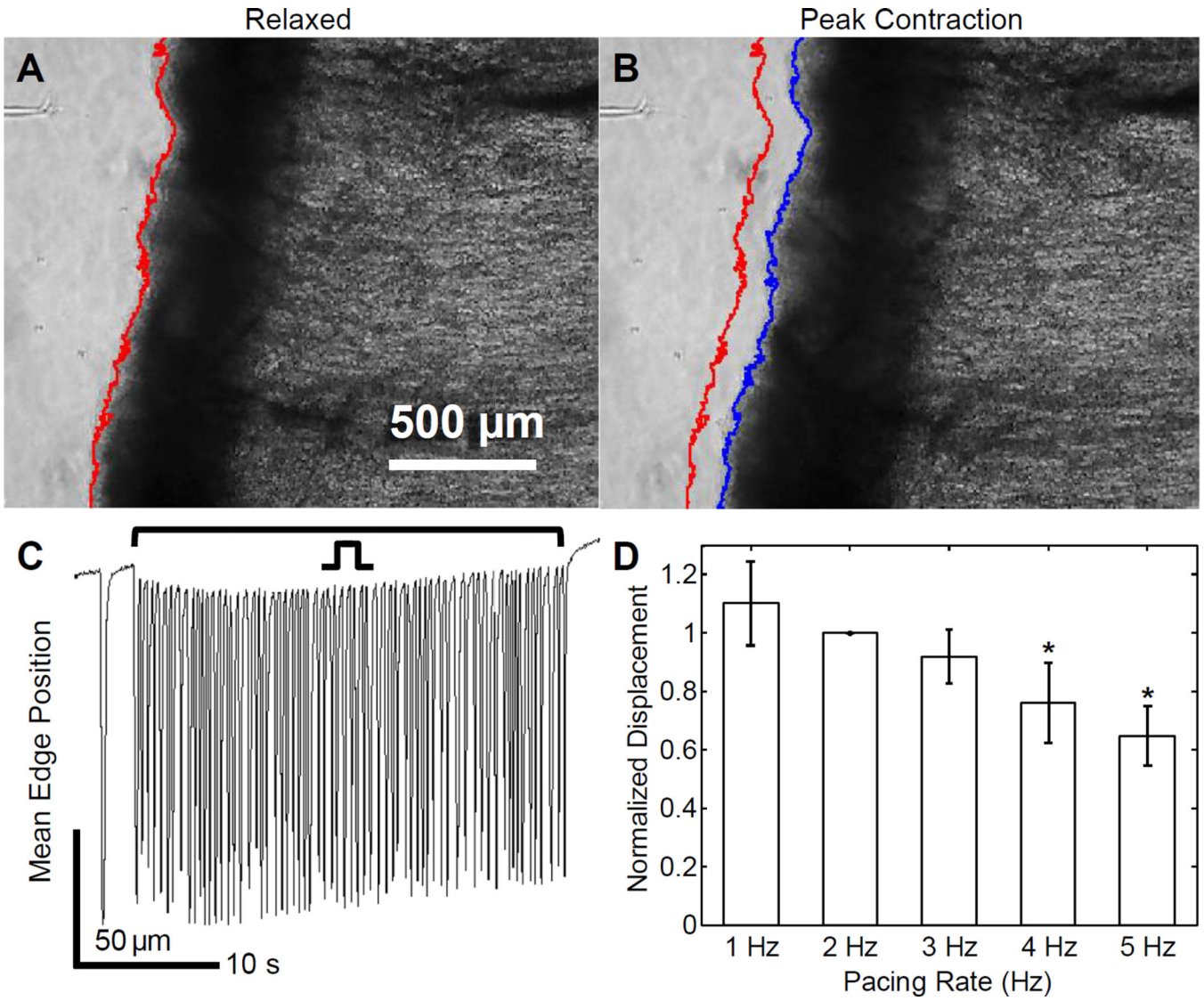

Fig. 6.

Contraction of EHS made from pig ECM. Representative images of EHS while relaxed (A), and at the peak of contraction (B) show shortening of day 5 EHS with 2 Hz pacing. The edge of the slice is outlined during rest (red line) and at peak contraction (blue line). The average slice displacement during each frame of the video recording was calculated, as shown over a 38 s recording interval (C), and from this mean contraction amplitude was quantified. The average force-frequency relationship across multiple EHS (n = 4–6 for each rate) is shown, normalized for each EHS to its 2 Hz peak displacement (D). * in D indicates significant decrease ($p < 0.05$) in contraction amplitude from that at 2 Hz. See Supplementary Video 3. (For interpretation of the references to color in this figure caption, the reader is referred to the web version of this article.)

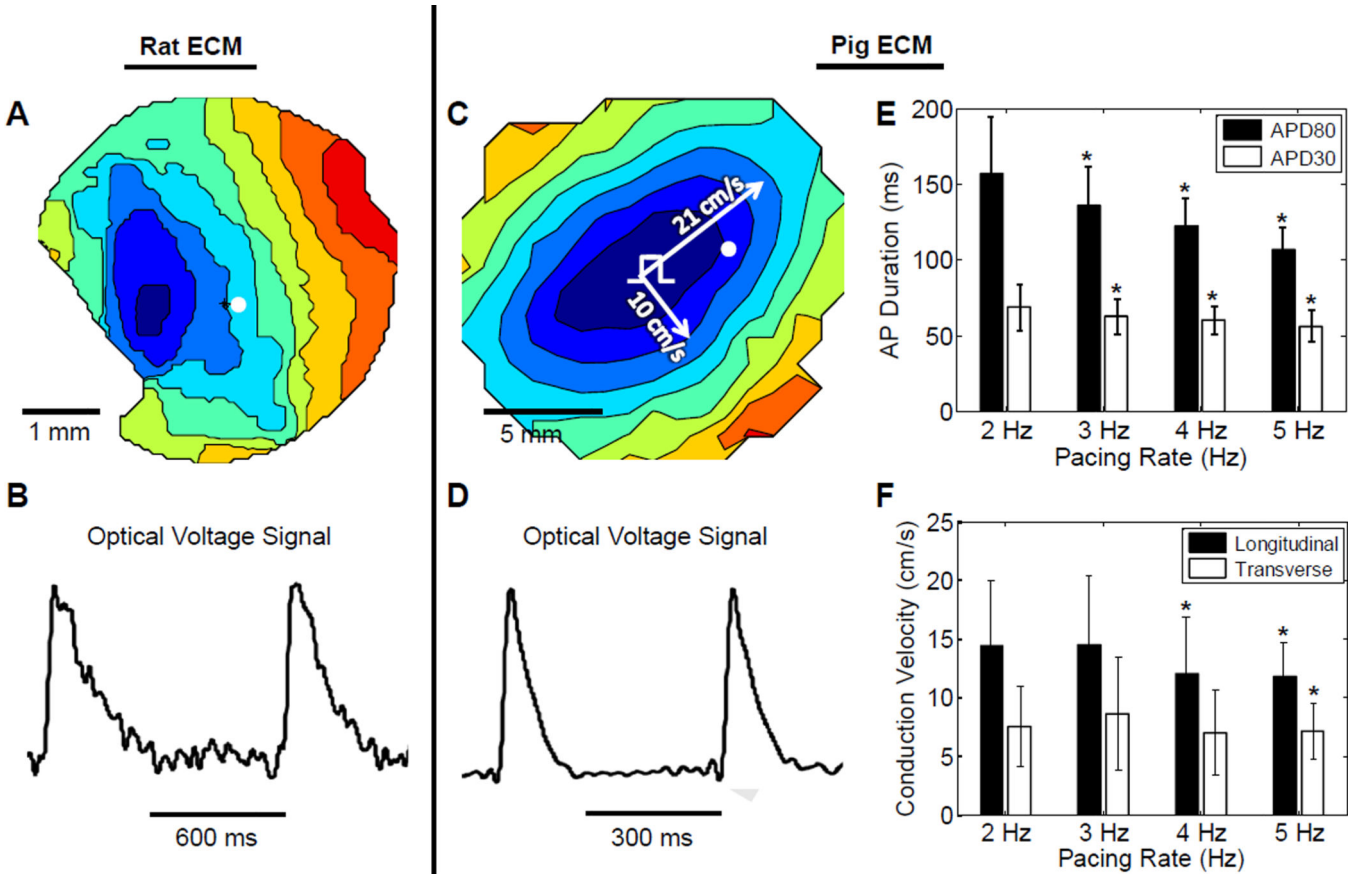

Fig. 7.

Optical recordings of transmembrane voltage in EHS made from rat and pig ECM. EHS from rat and pig ECM were optically mapped with voltage-sensitive dye after 5–7 days in culture. Activation maps (A) and signal traces (B) show anisotropic propagation in EHS from rat ECM during 1 Hz field stimulation. Signal in B is from location marked by white dot in A. Activation map (C) for EHS from pig ECM showed anisotropic propagation during 2 Hz point stimulation. Activation maps in A and C have 10 ms isochrones and same color scale. White pulse symbol indicates site of the stimulus electrode. White dot marks location of recording in D. White lines and values show the calculated longitudinal and transverse conduction velocity (CV) vectors. Optical voltage signals in EHS (D) showed normal action potential morphology, and APD_{80} and APD_{30} were measured at different pacing rates (E). CVs in the longitudinal and transverse directions were measured at different pacing rates (F). In E–F, the number of EHS recorded was 17,15,13 and 7 at pacing rates 2–5 Hz, respectively, with fewer samples at faster rates due to loss of 1:1 capture. * in E and F indicates significant change ($p < 0.05$) from values at 2 Hz. See Supplementary Video 4, corresponding to C and D. (For interpretation of the references to color in this figure caption, the reader is referred to the web version of this article.)

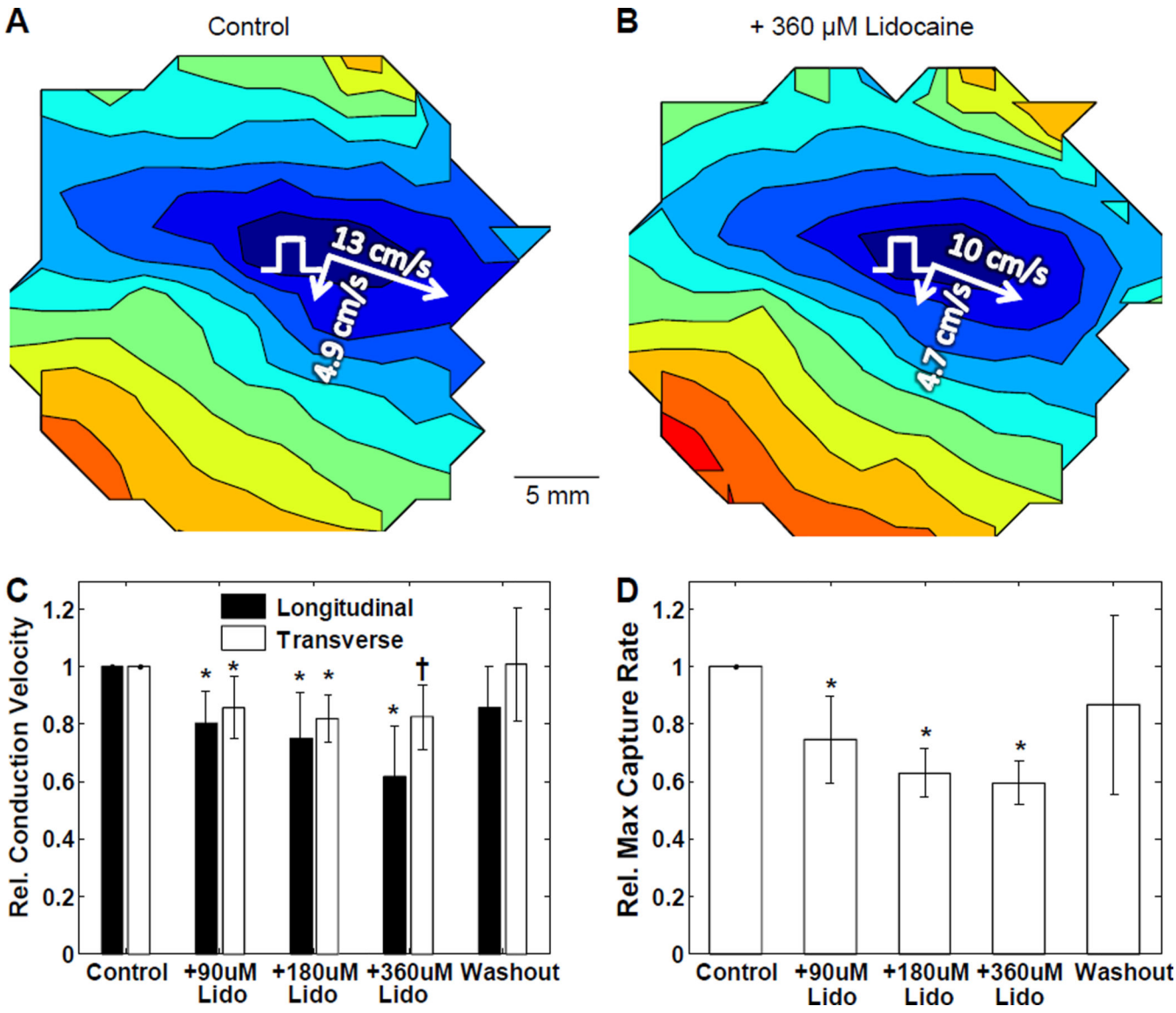

Fig. 8.

Response of EHS made from pig ECM to lidocaine. Activation maps in the absence (A) and presence (B) of 360 μM lidocaine at 2 Hz pacing rate showed lidocaine caused conduction slowing in EHS. Activation maps in A and B have 20 m isochrones and the same color scale. White pulse symbol indicates site of the stimulus electrode. White lines and values show the calculated longitudinal and transverse conduction velocity vectors. When normalized to lidocaine-free control (longitudinal CV = 10.3 ± 3.1 cm/s, transverse CV = 4.0 ± 0.8 cm/s, and max. capture rate = 4.1 ± 1.2 Hz), lidocaine decreased transverse and especially longitudinal CV (2 Hz pacing shown) (C) and maximum capture rate (D) in a dose-dependent manner that was largely reversed after at least 15 min washout. * in C and D indicates significant difference ($p < 0.05$) from control (i.e. 1). † in C indicates significant difference ($p < 0.05$) from relative CV in longitudinal direction. n = 4–5 EHS in C and D; one EHS in C lost capture in 360 μM lidocaine. (For interpretation of the references to color in this figure caption, the reader is referred to the web version of this article.)

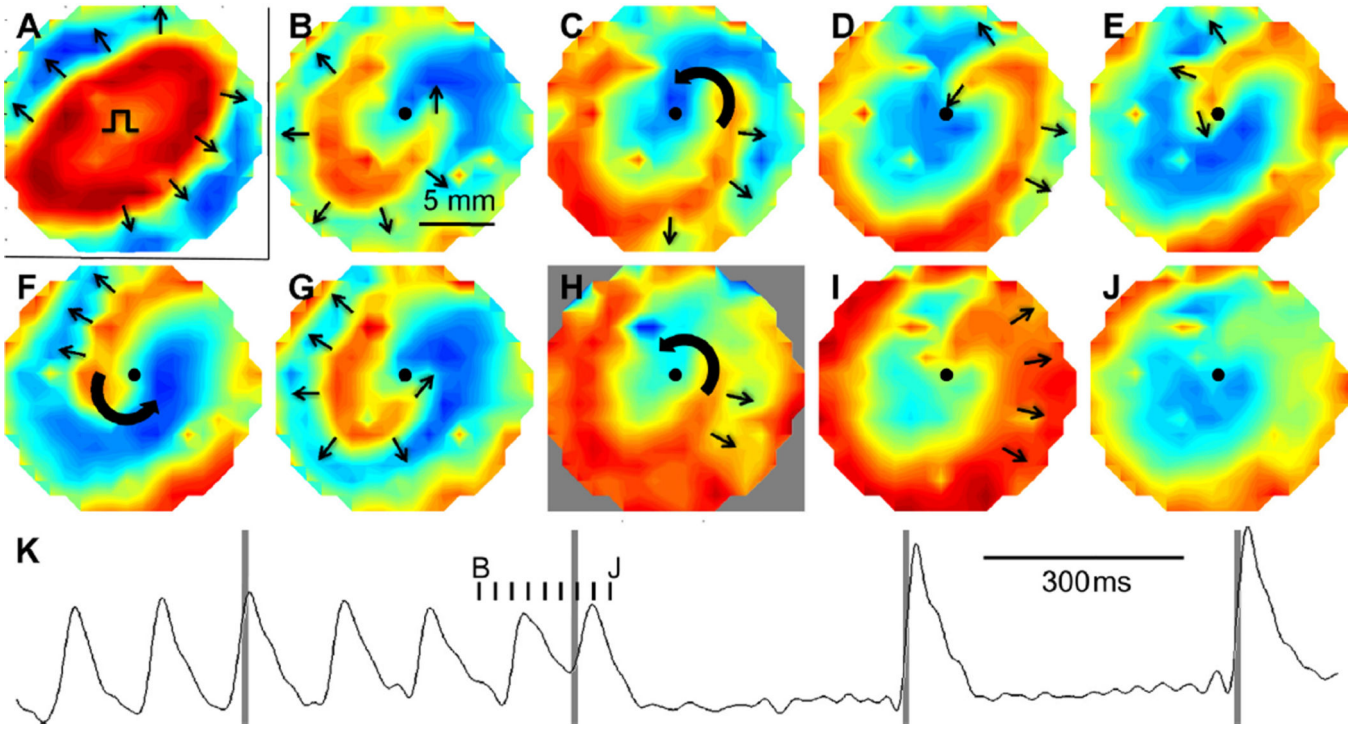

Fig. 9.

Reentrant activity in EHS made from pig ECM. EHS produced uniform anisotropic conduction at 2 Hz pacing rate (A). Pulse symbol indicates site of the stimulus electrode. A counterclockwise spiral wave was induced after pacing at 8.3 Hz. Voltage maps taken 25 ms apart show reentry (B–G). Four 24 V/cm electrical shocks were applied 500 ms apart, and the second (H, gray background) terminated the spiral wave (I–J). Small arrows show movement of AP wavefront. Thick curved arrows show propagation around the central rotation of the spiral wave. K shows the entire sequence of applied shocks (gray lines) and the optical voltage recording from the location marked by the small black dot in B–J. Small black tick marks indicate when the snapshots in B–J were taken. See Supplementary Video 5.